PROCEEDINGS A

royalsocietypublishing.org/journal/rspa

Research

Cite this article: Chaudhary G, Niu L, Han Q, Lewicka M, Mahadevan L. 2023 Geometric mechanics of ordered and disordered kirigami. *Proc. R. Soc. A* **479**: 20220822. https://doi.org/10.1098/rspa.2022.0822

Received: 6 December 2022
Accepted: 20 April 2023

Subject Areas:
materials science, structural engineering, applied mathematics

Keywords:
kirigami, geometric mechanics, origami, thin sheets

Author for correspondence:
L. Mahadevan
e-mail: lmahadev@g.harvard.edu

Electronic supplementary material is available online at https://doi.org/10.6084/m9.figshare.c.6631833.

THE ROYAL SOCIETY PUBLISHING

Geometric mechanics of ordered and disordered kirigami

G. Chaudhary[1], L. Niu[2], Q. Han[3], M. Lewicka[4] and L. Mahadevan[1,2]

[1]School of Engineering and Applied Sciences, Harvard University, Cambridge, MA 02138, USA
[2]Department of Physics, Harvard University, Cambridge, MA 02143, USA
[3]Department of Mathematics, University of Notre Dame, South Bend, IN 46556, USA
[4]Department of Mathematics, University of Pittsburgh, Pittsburgh, PA 15260, USA

ML, 0000-0002-9717-7499; LM, 0000-0002-5114-0519

The presence of incomplete cuts in a thin planar sheet can dramatically alter its mechanical and geometrical response to loading, as the cuts allow the sheet to deform strongly in the third dimension, most beautifully demonstrated in kirigami art-forms. We use numerical experiments to characterize the geometric mechanics of kirigamized sheets as a function of the number, size and orientation of cuts. We show that the geometry of mechanically loaded sheets can be approximated as a composition of simple developable units: flats, cylinders, cones and compressed Elasticae. This geometric construction yields scaling laws for the mechanical response of the sheet in both the weak and strongly deformed limit. In the ultimately stretched limit, this further leads to a theorem on the nature and form of geodesics in an arbitrary kirigami pattern, consistent with observations and simulations. Finally, we show that by varying the shape and size of the geodesic in a kirigamized sheet, we can control the deployment trajectory of the sheet, and thence its functional properties as an exemplar of a tunable structure that can serve as a robotic gripper, a soft light window or the basis for a physically unclonable device. Overall our study of disordered kirigami sets the stage for controlling the shape and shielding the stresses in thin sheets using cuts.

1. Introduction

Kirigami, the art of paper cutting to create an articulating single sheet, is now increasingly viewed as a paradigm for the design of mechanical metamaterials that exhibit exceptional geometric and structural properties [1–3]. The basis for kirigami is the well-known observation that the mechanical response of thin sheets is characterized by the scale separation induced by slender geometries, which makes bending deformations inexpensive compared to stretching deformations. In kirigami, varying the number, size and location of cuts provides extra degrees of control via the internal localization of large bending deformations anchored at the ends of the cuts. This raises a number of questions associated with both the forward problem of understanding the mechanics of these topologically and geometrically complex materials, as well as the inverse problem of designing the cuts to obtain different types of articulated deformations for shape optimization. Recent work in the context of the forward problem has focused primarily on the mechanics of kirigami with simple distributions of periodic cuts, aimed at characterizing the response using a combination of theory, experiment and computation [4–6]. By contrast, the inverse problem of designing cuts that allow for articulated shape transformations has been limited primarily to geometric optimization [7,8], without much discussion of the mechanical response of the resulting structures by incorporating bending energies. To design cut patterns to control the shape and response of kirigamized sheets, we need to combine aspects of both these classes of problems by understanding the geometric mechanics of sheets with multiple aperiodic cuts. Here, we take a step in this direction by characterizing the geometry and mechanics of a single cut subject to deformation, and then generalize our study to kirigami sheets with randomly located cuts, but staying in the dilute limit where the cuts do not intersect.

2. Geometry and mechanics of a sheet with a single cut

To get a sense of the geometry of deformations in a kirigamized sheet, in figure 1, we show a sheet with four parallel cuts that has been strongly stretched, leading to a shape like a kabuki mask. In figure 2*a*, we show the shape of a thin circular sheet of radius R, thickness h and a single horizontal cut of length l. When the nominal strain γ induced by the applied horizontal force crosses a threshold, the initially planar sheet buckles out of the plane into a complex geometrical shape. Casual observations of the sheet show that the deformed sheet is constituted of simple conical and cylindrical domains connected by transition regions, as expected from thin sheet mechanics; increasing the topological complexity of the sheet increases the number, size, shape and orientational order of such domains.

We use experimental observations and numerical simulations to study the geometrical mechanics of kirigamized sheets (see electronic supplementary material, S2), starting from the nonlinear elastic energy of a triangulated plate that is minimized using a conjugate gradient method. In our simulations, cuts are defined as thin rectangular slits of length l and small width w, with a semicircular tip of diameter w added to the ends of each cut.

Figure 2*a* shows the mean curvature of the simulated sheet for different values of the strain γ when the cut is initially orthogonal ($\theta = \pi/2$) to the loading axis (the line connecting the loading points O_1 and O_2, the separation of which defines the strain γ) (figure 2*a*(i)). We observe that for very low strains $\gamma \ll 1$, the sheet stretches, but remains planar. When γ exceeds a critical value γ_c, the sheet buckles with bending deformations becoming localized along two conical domains centred near each end of the cut, and a large cylindrical domain of nearly uniform mean curvature κ appears to connect the cut ends and the loading points on both sides. Further stretching of the sheet causes an increase in the curvature of these cylindrical domains, and reduces the Euclidean distance between the end-points (A and B) of the cuts from its initial length (see electronic supplementary material, movie S1). This deformation localization enables the three-dimensional straightening of geodesics, the minimal-length curves connecting the loading points O_1, O_2 that

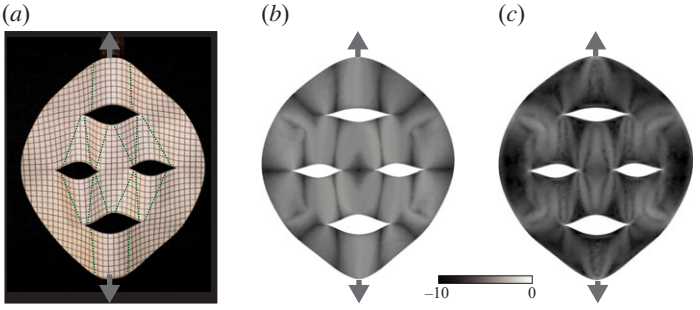

Figure 1. Complex response of a stretched kirigami sheet with four parallel cuts. (*a*) When a thin circular paper sheet ($R = 8.9$ cm, $h = 0.01$ cm) with several cuts is loaded along diametrically opposite ends, it buckles into a complex three-dimensional surface that can be geometrically approximated by a set of cylindrical sections and cones emanating from the ends of each cut. (*b*,*c*) The simulated energetic decomposition of the sheet reveals that the dominant energetic contributions stem from the quasi-cylindrical regions connecting the cuts, whose widths scale with the lengths of the cuts they connect. Brightness corresponds to a logarithmically scaled energy (details are in the electronic supplemental material). (*a*) Kirigami sheet, (*b*) bending energy, (*c*) stretching energy.

do not cross any cuts, shown in figure 2*a*,*b*; details of the geodesic construction and behaviour are described in §4.

Simultaneously, the free edges associated with the cut deform into a shape that resembles Euler's elastica [9] as shown in figure 2*c*. When the applied strain becomes very large, the end points of these elasticae, corresponding to the ends of the cut, come together consistent with the geodesics straightening in three dimensions. If the sheet thickness is very small ($h/R \to 0$), the bending energy of the sheet becomes negligible relative to the stretching energy, and any deformations must become approximately isometric. Based on our observations, we expect that in this limit, the sheet will approach a flat folded state, a configuration discussed in §4.

Moving from this geometric description of the sheet to its mechanical properties, the force–displacement response of the kirigami sheet described in figure 2*a*–*c* is shown in figure 2*d*. At low values of strain γ, the force is linearly proportional to γ, but once the sheet buckles, the force plateaus as the sheet deforms by bending out of the plane. Eventually, as the ends of the cut come together, the sheet stiffens as it cannot deform any further without significant stretching and the force increases, showing a divergent behaviour. In the buckled state, there are two alternate modes of deformation: a symmetric mode when both cylindrical domains on either side of the cut are in-phase, and an antisymmetric mode where both cylindrical domains on either side of the cut are out-of-phase. The plateau force for these two cases differs marginally, but the linear and the divergent responses away from the plateaus are indistinguishable as can be seen in figure 2*d*.

To understand the origin of this divergence, we use a scaling approach. The torque due to the applied force f acting over a length S corresponding to the (small) distance between the ends of the cut is balanced by the internal elastic torque $B\kappa_c$ where κ_c is the characteristic mean curvature in the neighbourhood of the end of the cut, with B as the flexural modulus of the sheet, so that $fS \sim B\kappa_c$. As shown in figure 3*b*, at the ends of the cut of small width w, the characteristic curvature $\kappa_c \sim \theta_c/w$, where θ_c is the angle at the cut's corner. As the sheet is pulled apart by the forces so that the cut edges are $2R\gamma$ apart at their widest, geometry implies that $\theta_c S/2 \sim 2R\gamma$ and $S \approx 2\sqrt{(l/2)^2 - 2R^2\gamma}$. Substituting these geometric relations into the overall torque balance then yields the relation

$$f \sim \frac{B}{wR}\frac{\gamma}{(\bar{l})^2 - \gamma}, \tag{2.1}$$

where $\bar{l} = l/(2\sqrt{2}R)$. Writing the stretch ratio of deformation as the end-to-end displacement $R(1+\gamma)$ normalized by the length of the shortest segment connecting the force application points to the ends of the cut, i.e. the piecewise linear geodesic length $l_g = 2\sqrt{(l/2)^2 + R^2}$, equation (2.1) can be

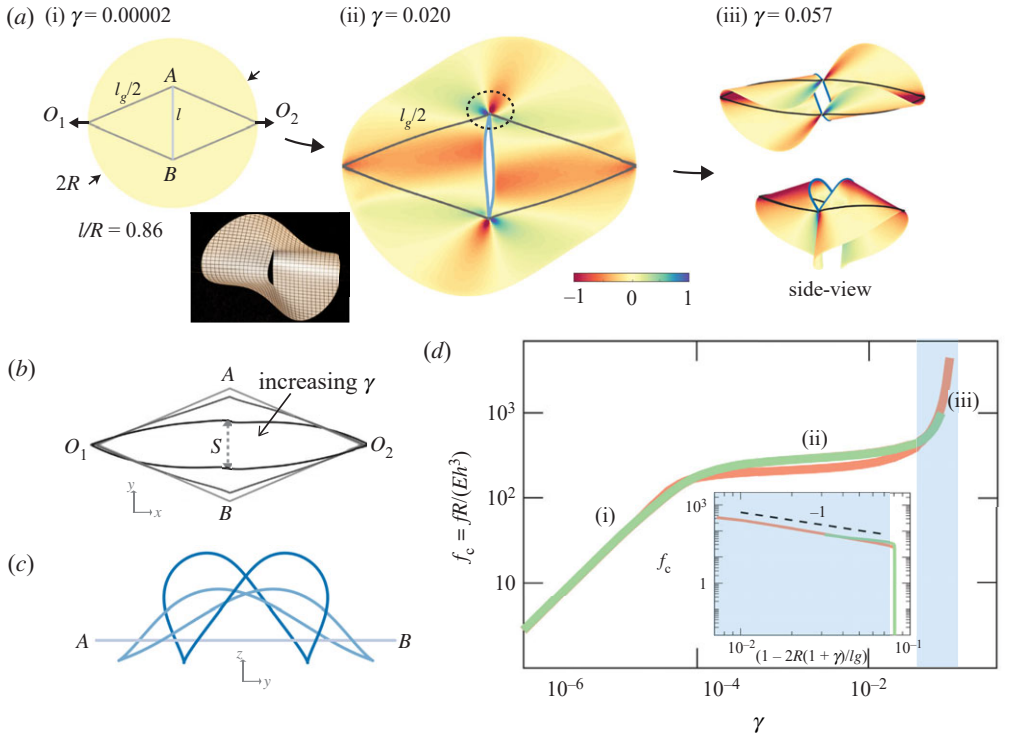

Figure 2. Geometric and mechanical response of a kirigami sheet with a single cut. (*a*) The simulated mean curvature of a sheet with a single cut along AB with two extensile point loads at O_1 and O_2 for various applied strains γ. The cut has length $l = 0.86R$ and is symmetric with respect to the centre of the sheet. Here, grey/black lines track the geodesics (length l_g) that connect the loading points without intersecting the cuts, and the blue lines track the cut shape. Highly localized bending deformations, as indicated by the mean curvature, can be observed at the edges of the cut. An experimental image (left, black background) shows a similar geometry. (*b*) Geodesic connecting the loading points O_1, O_2, extracted from (*a*), tend to align with the axis O_1O_2 with increasing strain. (*c*) The evolving shape of the cut edges is similar to an elastica [9]. Here, the cut boundary is extracted from (*a*), and darker colour shows the cut shapes at higher strains. (*d*) Numerically obtained force displacement curves for the case shown in (*a*). The curves show three distinct regimes corresponding to the cases shown in (*a*). The green curve corresponds to the configurations shown in (*a*), while the red curve corresponds to the case where the two cut edges buckle out-of-plane in opposite directions. Inset: a log-log plot of the scaled strain plotted against the force shows a form similar to the response of a freely jointed chain with the same divergent force–strain behaviour. The shaded region in the inset corresponds to the shaded region in the main figure.

expressed in a more familiar form $\hat{f} \sim 1/(1 - 2R(1 + \gamma)/l_g)$ where $\hat{f} = f/(BwR)$ which we see is the same as the divergent response of a freely jointed polymer chain [10]. The inset to figure 2*d* shows that the mechanical response with the rescaled definition of the stretch agrees well with this simple scaling estimate. We pause to make two comments: (i) the divergent mechanical response of freely jointed chain is intimately linked to the balance between entropic effects and a finite chain length, quite unlike the divergent response of the athermal kirigami sheet, which is due to the localization of curvature of the sheet at the ends of the cut and (ii) the geometric origin of the divergent behaviour suggests that single-cut kirigami can serve as a building block for a new type of lockable mechanical response [11] that is material independent, and can instead be controlled by geometry and topology.

Having understood the geometry and mechanical response of a sheet with a single symmetrically placed cut, we ask what would happen when the cut's length l and/or orientation θ is varied. Figure 3*a* inset shows the mechanical response for various cases where l is varied

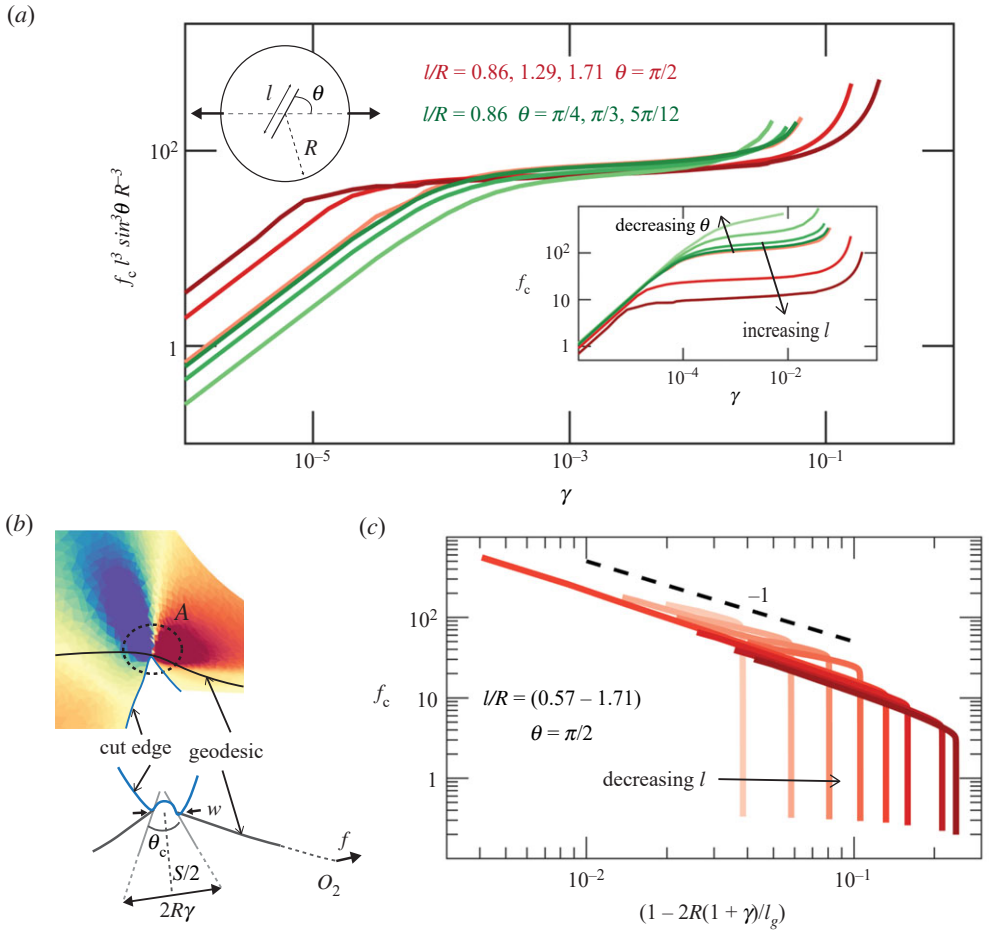

Figure 3. Mechanical response of a kirigami sheet with an angled cut. (*a*) Scaling of the stretching force for a sheet of radius R with a single cut with the parameter $R^3/(l^3 \sin^3\theta)$ collapses the plateau regions of the mechanical responses for the cases of varying cut length l and orientation θ. Unscaled data are shown in the inset. Red curves correspond to the cases with $\theta = \pi/2$ and $l/R = 0.86, 1.29, 1.71$. Green curves are the cases with $\theta = \pi/4, \pi/3, 5\pi/12$ and $l/R = 0.86$. (*b*) A zoomed in view of the cut corner for the case (figure 2*a*(iii)), and a schematic showing the relevant length scales that govern the mechanics in this regime (see text for further details). (*c*) Strongly strained kirigami sheets qualitatively show a 'freely jointed' polymer-chain like divergence as the length $\langle O_1O_2\rangle \to l_g$. Shown here are the cases with $\theta = \pi/2$ and $l/R \in [0.57, 1.71]$.

keeping the cut orientation orthogonal to the clamped axis ($\theta = \pi/2$) in red curves. The mechanical response in all cases is qualitatively similar to figure 3*a*, with a shift in the applied strain γ at the onset of plateau response, the magnitude of the plateau force, and the strain at the onset of divergent response. Larger l results in a lower value of the threshold in γ and a lower force plateau persisting for longer, before the force diverges. Similarly, changing the orientation θ of the cut changes the mechanical response by increasing the plateau force value, as the initial cut direction is more aligned with the direction of the clamping axis. The deformed geometric configurations for all these cases are shown in electronic supplementary material, figure S3.

To quantify these observations, we note that the linear response at very small strain corresponds to the planar stretching of sheet. We note similarities of our scaling analysis to previous studies [4,12,13], and hence keep the discussion on the linear regime and the onset of the nonlinear response very brief here. The presence of the cut leads to a stress intensification near the ends of the cut. As first described in Inglis' seminal work [14], the stress near the tip of

a cut of length $2l$ and a very small radius of curvature w can be approximated as $\sigma_0\sqrt{l/w}$, where σ_0 is the far field applied stress on a large plate. Assuming that the planar elastic deformation is confined near the cut tip, we get $\sigma_0\sqrt{l/w} \sim E\gamma$. Hence we expect $\sigma_0 \sim f \sim 1/\sqrt{l}$ (see electronic supplementary material, figure S2b). Following the initial linear increase in the force with applied strain, the sheet buckles when the compressive load on a plate of size corresponding to the length of a cut reaches a threshold given by the buckling stress $\sigma_b \sim B/hl^2$, with B being the flexural rigidity of the sheet, so that the buckling force $f_b \sim (B/h^2R)(1/l^2)$ (see electronic supplementary material, figure S2d). Then the strain at which the sheet buckles (γ_b) can be estimated from a balance of the in-plane stress ($\sim E\gamma_b/\sqrt{l/w}$) with the buckling stress, so that $\gamma_b \sim 1/(l/R)^{3/2}$ (see also electronic supplementary material, figure S2c).

Following the onset of buckling, for small out-of-plane displacements $\delta \ll l$ of the cut boundary, the curvature of the deformed cylindrical core of the sheet scales as $\kappa \sim \delta/l^2$. Thus the total bending energy of the sheet scales as $U \sim Eh^3\kappa^2 A \sim Eh^3\delta^2 R/l^3$, with $A \sim Rl$ being the area of the quadrilateral O_1AO_2B shown in figure 2*a*. Further, the out-of-plane displacement can be expressed as $\delta \approx R\gamma^{1/2}$, and hence $U \sim Eh^3R^3\gamma/l^3$. Thus the force scales as $f = \partial U/\partial(R\gamma) \sim Eh^3R^2/l^3$ (see electronic supplementary material, §S3 and figure S1). For a cut oriented at an arbitrary angle θ to the clamped axis, we replace l by its orthogonal projection to the loading axis $l\sin\theta$. Figure 3*a* shows the collapsed data from figure 3*a* inset, indicating that the bending energy localization in the elasticae corresponding to the two edges of cut determines the magnitude of plateau response in the force–displacement curves. We note that we have ignored the contribution of energy from the conical domains since the size of conical domains is much smaller than the cylinder-like domains just above the onset of out-of-plane deformation, and the mean curvature decays away from the cone tip as $\kappa \sim 1/r$. At large applied strain, when the geodesics are relatively better aligned with the loading axis, application of further strain induces a strong bending deformation at the cut corners. Sheets with a finite tearing threshold stress generally tear as a result of this deformation, and this raises a class of different questions about the nature and shape of the curve of tearing [15], which we do not discuss here. Figure 3*c* depicts the rescaled force–displacement curves showing the divergence response of sheets with varying cut length, which agree well with the scaling arguments given by equation (2.1).

3. Geometry and mechanics of a sheet with multiple cuts

We now turn to understand how the geometric mechanics of single-cut kirigami translates into our understanding of sheets with multiple cuts. In figure 4*a*, the mean curvature maps of the deformed sheet show the similarity in the localized deformation for the different cases with the number of cuts N, all of which are perpendicular to the loading axis, varying from 2 to 12 (see electronic supplementary material, movie S2 and figure S6). We see that the deformed geometry in all cases consists of four conical domains, and $N+1$ connected elasticae N. Indeed, regardless of the number of cuts, the conical domains localize to the ends of cuts that are nearest to the loading points while the sheet remains flat in between. Figure 4*b* shows the mechanical response of sheets kirigamized with varying number of cuts and shows that increasing the number of cuts softens the system, reducing the plateau force and delaying the transition to the ultimately divergent force–displacement response.

To characterize the mechanical response in the case with multiple cuts, we approximate the bending deformations as localized in $N+1$ elasticae close to the onset of out-of-plane deformation so that the elastic energy $U \sim Eh^3R^2d\gamma/l^3$, and hence the force $f \sim \partial U/\partial(R\gamma) \sim Eh^3Rd/l^3$, where d is the distance between the loading point and the nearest cut (see electronic supplementary material, §S3 and figure S4). Consistent with this, rescaling the force with d collapses the data over the scale of intermediate deformations as shown in the inset of figure 4*b*.

At large strains, the strong bending deformations near the cone tips appear similar to the case with a single cut discussed earlier. Predicting the potential sites of structural failure in practical applications requires knowledge of the location of conical domains. Our observations suggest

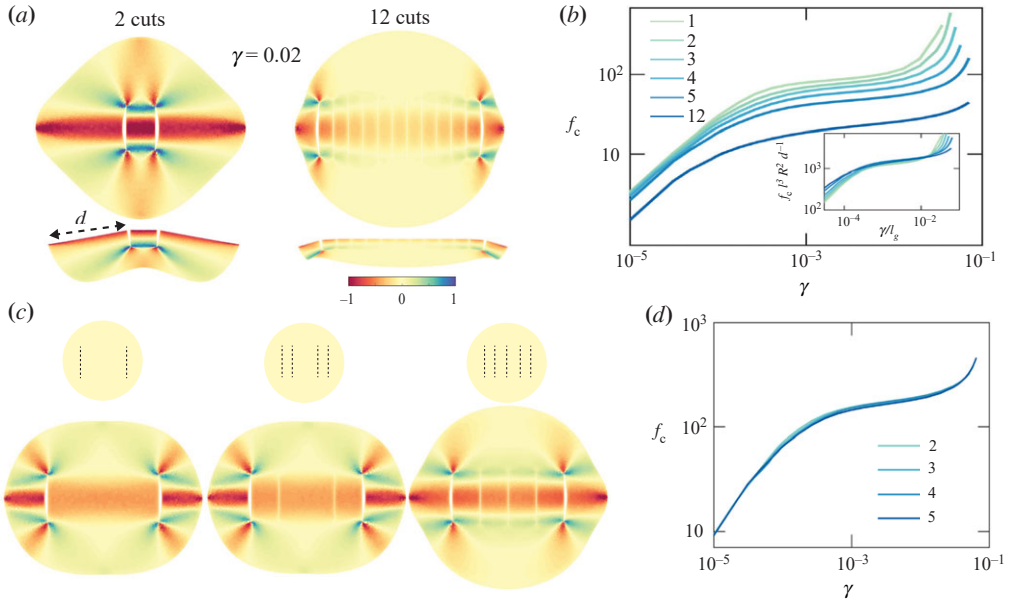

Figure 4. Geometric and mechanical response of a kirigami sheet with multiple parallel cuts. (*a*) Localized bending deformation in sheets with multiple cuts aligned perpendicular to the loading axis shows similar geometric structures regardless of the number of cuts. Shown are top and side views of the cases with 2 and 12 cuts. (*b*) Mechanical response for kirigami sheets with different number of parallel cuts ($\theta = \pi/2, l = 0.57R$). (inset) Rescaled force with the length d, labelled in (*a*) collapsed the plateau regime. (*c*) Effective shielding of the inner cuts due to the localization of bending deformation near the outer cuts that are closest to the loading points is demonstrated. The conical domains are absent in the additional cuts added to the configuration in the left case. (*d*) Mechanical response for the cases shown in (*c*) show that the mechanical response in the linear and plateau regime is essentially the same and only the cuts nearest to the loading points determine the stiffness of the kirigamized sheet in these regimes.

that the high-stress conical domains will appear at the ends of a particular cut, if the presence of that cut increases the geodesic length l_g. To formalize this, we define a binary participation ratio (PR) for each cut as

$$\mathrm{PR}_i = \begin{cases} 1 & \text{if } l_g^0 > l_g^{-i}, \\ 0 & \text{if } l_g^0 = l_g^{-i}, \end{cases} \tag{3.1}$$

where l_g^0 is the geodesic length evaluated for a given arrangement that includes cut i, and l_g^{-i} is the geodesic length with the ith cut removed from the arrangement. For the cases shown in figure 4*a*, the two cuts nearest to the loading points have a PR = 1 and all other cuts have PR = 0. Similarly, for the cases with two cuts of varying projected lengths (see electronic supplementary material, figure S5), conical domains disappear at the corners of cuts with PR = 0. In figure 4*a*, we see that an increase in the number of cuts increases the geodesic length l_g. Since the divergent force–displacement response emerges as $2R(1+\gamma) \to l_g$, the plateau response in the force–displacement curves is observed at larger γ for larger N. In cases with $N > 2$, fixing the location of the cuts closest to the points of force application sets the trajectory of geodesics as well as the geodesic length l_g, regardless of the presence of the inner cuts. In figure 4*c*, we see that the mean curvature field of the kirigamized sheets with different cut configurations results in similar profiles. Each case has two conical domains that appear at the corners of the cuts closest to the points of force application, a cylindrical core extending between the two loading points whose extent is defined by the cut length. Since the geodesic length is the same for all the cases in figure 4*c*, the divergent response occurs at the same strain regardless of the presence of the inner cuts; in fact,

the force–displacement curves overlap at all applied strains for such cases, and the geometry of the deformed sheets is almost identical as shown in figure 4*d*.

When cuts are distributed in a disordered manner on a loaded sheet, the geometry of the geodesics continues to control the mechanical response of the overall system. In figure 5*a*, we show an example with 21 cuts of the same length (totaling $8R$), with randomly chosen locations of the cut midpoint and its orientation, but with a minimum separation between the cuts and between the cut and the loading points. The localization of deformation in participating cuts' elasticae and conical domains is evident, while the sheet remains flat and undeformed near cuts with PR = 0 (also see electronic supplementary material, figure S7).

To obtain the average response for the case of disordered kirigami, we repeat the simulations keeping the sum $\sum l$ constant. Figure 5*d* shows the mechanical response for these disordered kirigami structures averaged over 10 samples per case. The overall nature of the force–displacement curve is similar to that of a single cut, with the plateau force decreasing for longer cuts. When the sum of the cut lengths $\sum l$ is small, we see a very weak deviation from the initial linear response, but with increasing $\sum l$ a clear plateau is observed. The divergent force–displacement response is observed when the geodesic connecting the two loading points nearly straightens out under applied strain, and we observe relatively large variance in force beyond the initial linear response due to the strong dependence on the cut length and location. Increasing the number of cuts while keeping $\sum l$ constant results in similar observations (see electronic supplementary material, figure S8) with a lower number of longer length cuts resulting in a lower plateau force response and an increased variance.

Since the cuts with PR = 0 do not significantly affect the geometric mechanics of the sheet, simply removing them from the given cut arrangement results in a sheet with a nearly identical geometric and mechanical response to a sheet with a much smaller number of cuts. In figure 5*b*, we show a kirigami pattern derived from that shown in figure 5*a* where the cuts with PR = 0 are removed. When such a structure is loaded, we see that the mean curvature field is quantitatively similar to that in figure 5*a*; indeed figure 5*c* shows that the force-strain curves are nearly the same.

It is evident from the observed geometry of disordered kirigami that the dominant modes of deformation become localized near a few cuts. Disordered cuts behave similarly to structured cuts, where the mechanical response depends on the distance of the cut from the loading point(s), its projected length, and its PR. At the onset of the buckling transition from the initial planar stretching response at very low strains, each cut with PR = 1 introduces a soft bending deformation mode in the sheet with a characteristic bending force f^*, given by the smallest buckling load, i.e.

$$f^* \sim Eh^3 \min_i \left[\frac{d_i}{l_i^3 \sin^3 \theta_{d_i}} + \frac{2R - d_i}{l_i^3 \sin^3 \theta_{2R-d_i}} \right] 2R, \tag{3.2}$$

where d_i is the minimum distance of the mid-point of the cut of length l_i from the loading points, and $2R - d_i$ is the distance of the cut midpoint from the farthest loading point, and θ_{d_i} and θ_{2R-d_i} are the angles that the cut makes with the line joining the midpoint of the cut to the points of force application. The above result follows from the assumption that at the onset of the plateau regime, the characteristic mean curvature for bending localization is set by the cut that corresponds to f^*, so that the two terms in equation (3.2) follow from the energy of two elasticae that exist on both sides of the cut. Here, we note that the cuts with PR = 0 do not alter the plateau response near its onset as seen with the cases in figures 4*b* and 5*c*. These observations allow us to determine the rescaled mechanical response shown in the inset of figure 5*d*, providing a reasonable collapse in the plateau region of force–displacement data. The spread in the scaled data is likely due to the simplification that the area of the sheet where energy is localized is assumed to span the sheet (hence the factor $2R$ in equation (3.2)), and that additional cuts which buckle following the onset of first buckling also contribute to localizing the bending deformation. All together, this allows us to reduce a given disordered kirigamized sheet to a simpler 'mechanical equivalent'

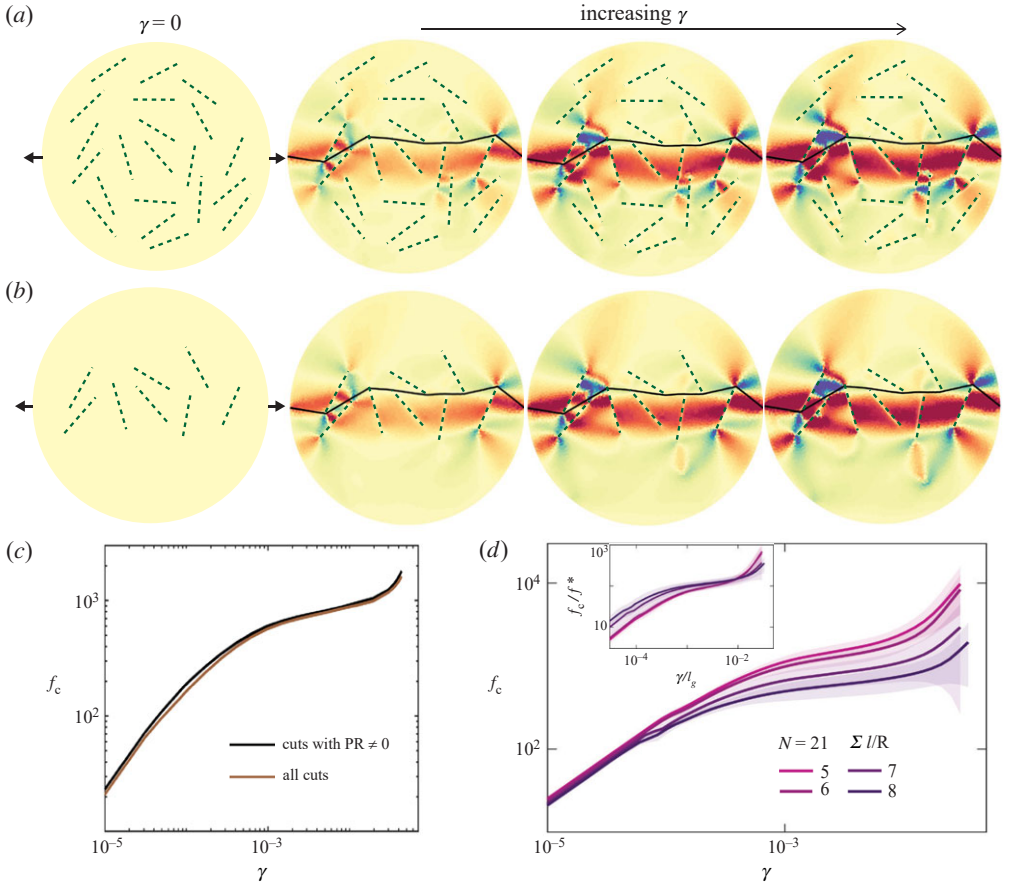

Figure 5. Geometric and mechanical response of a kirigami sheet with disordered cuts. (*a*) Localized deformation in a disordered kirigami sheet of radius *R* with 21 randomly distributed cuts of same individual length (dashed lines) with a total length 8*R*. The mean curvature of the deformed sheet is projected on the initial flat configuration. With increasing strain the mean curvature of the domains where the bending deformations are localized generally increases. Note that only a few cuts which directly impact the geodesic path connecting the points of force application, shown in solid black curve, localize the deformation near them. (*b*) Removing the cuts with PR = 0 (defined in equation (3.1)) from (*a*) doesn't significantly impact the deformed configuration of the kirigami structure; the majority of the localized bending domains are similar to that of (*a*). Most of the deformation is still determined by the cuts closest to the two ends, which cause the greatest deviation in the geodesic path. (*c*) The mechanical response of the structures in (*a*) and (*b*) with 21 and 8 cuts, respectively. The structure with 21 cuts has a slightly softer response in the linear regime while the plateau force values for both the cases are essentially the same. (*d*) Mechanical response of a disordered kirigamized sheet perforated with 21 randomly distributed uniform cuts, with varying total cut length has similar behaviour as sheets with single and multiple structured cuts. Inset: Rescaled force data (using equation (3.2)) collapses the plateau region reasonably well.

(e.g. figure 5*b*). Thus, our simple scaling approach reduces the complexity of disordered kirigami using elementary geometric mechanics.

4. Rectifying the geodesics and the flat-foldable kirigami

For an initially flat sheet, our observations suggest that the shortest path between the points of force application for simple cut patterns is just a polygonal curve that connects these points, i.e. geodesics in a planar sheet with random cuts are polygonal. When a very thin sheet is deformed by boundary forces, its ultimate shape is characterized by the formation of sharp

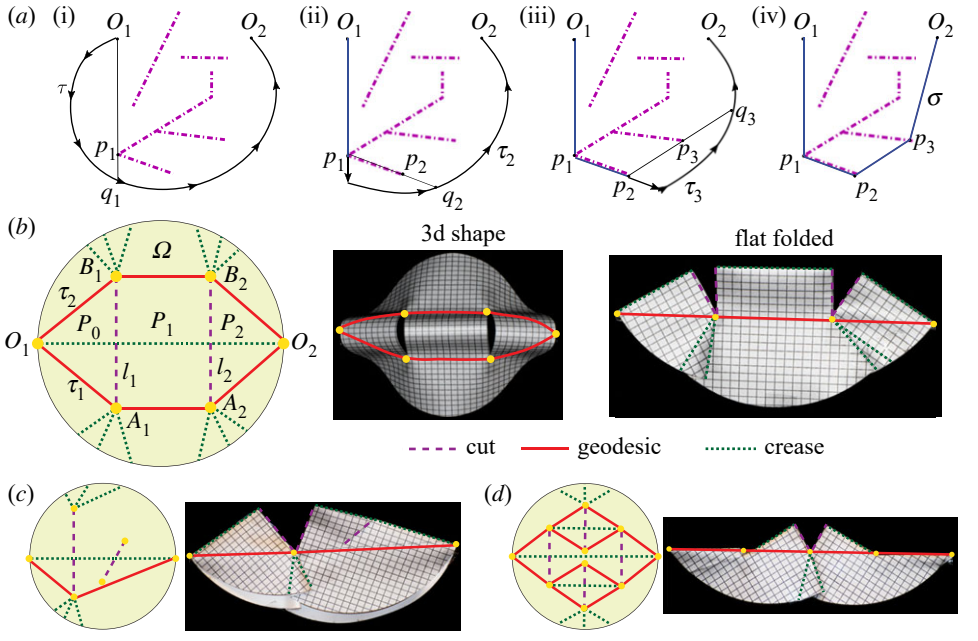

Figure 6. (*a*) (Adapted from [16].) The path-shortening algorithm yields a polygonal competing to be a geodesic. (*b–d*) Strongly stretched inextensible sheets of negligible bending rigidity, $h \to 0$, can be flat-folded to two-dimensional sheets while simultaneously rectifying all geodesics to lie along a single straight segment in space.

creases as the sheet folds on itself, as shown in figure 6*b–d*. These observations of the geometry of strongly deformed kirigamized sheets show that the polygonal geodesic in the plane become an approximately straight geodesic in $\mathbb{R}^3$ connecting the points of force application. The sheet can be then flat-folded, leading to a configuration that is a piecewise affine isometric immersion of the plane. We leave precise theorems and proofs of these statements for a separate study [16], but provide a brief summary of the results here.

(a) Polygonal structure of the geodesics

We represent the given set of cuts L, contained within an open, bounded, convex domain $\Omega \subset \mathbb{R}^2$, as the union of the edges of a graph G. Without loss of generality, G may be taken as planar, i.e. each pair of its edges intersects at most at a single common vertex. The polygonal structure of geodesics follows from the idea of a path-shortening algorithm (figure 6*a*). Given $O_1, O_2 \in \bar{\Omega} \setminus L$ and a piecewise C^1 curve $\tau : [0,1] \to \bar{\Omega} \setminus L$ with $\tau(0) = O_1$ and $\tau(1) = O_2$, one successively replaces its portions by segments, as follows. Firstly, for $t > 0$ sufficiently small, the segment $\overline{O_1\tau(t)}$ does not intersect L. Let $t_1 \in (0,1]$ be the first time that the segment $\overline{O_1\tau(t_1)}$ intersects L. If $\tau(t_1) = O_2$, then $\overline{O_1O_2}$ is the desired geodesic connecting O_1 and O_2. Otherwise, $\overline{O_1\tau(t_1)}$ must contain some of the vertices of the cuts. Call p_1 the closest one of these vertices to $\tau(t_1)$ and perform the concatenation of the segment $\overline{p_1\tau(t_1)}$ with the curve τ restricted to $[t_1, 1]$. The process is now repeated from p_1. After finitely many such steps one obtains a polygonal connecting O_1 and O_2, with a shorter length than τ.

(b) Geodesic rectification and flat foldability

The construction of the desired isometric immersion follows from the folding algorithm below that consists of three steps. Let $O_1, O_2 \in \partial\Omega$ and denote by l_g the length of the geodesics between O_1, O_2. Then, we start with two preparatory steps.

Step 1. Sealing portions of inessential cuts that do not affect l_g. To this end, label cuts (the edges of G) by $l_1, \dots, l_n$. Move the first endpoint vertex of l_1 toward its second vertex, and start "sealing" the portion of the cut l_1 left behind. The length of the geodesics connecting O_1 and O_2 may drop initially, in which case the configuration is left unchanged. Otherwise, the geodesic distance is continuously non-increasing, although it may initially remain constant. The sealing process is stopped when the aforementioned distance becomes strictly less than the original one, and the new position point is labeled as the new vertex endpoint of l_1. In the next step, the remaining endpoint is moved along l_1 toward the (new) first endpoint and the process is repeated, thus possibly sealing the cut l_1 further. The same procedure is carried out for each l_i in the given order $i = 1, \dots, n$. It follows that upon repeating the same process for the newly created configuration, labeled the *minimal configuration* will not be further altered. While different ordering of cuts and vertices may yield different minimal configurations and new geodesics may be created in the cut-sealing process, all original geodesics are preserved. Also, since the newly created set L is a subset of the original one, finding the isometric immersion relative to the new L will yield the desired isometric immersion.

Step 2: Ordering of the geodesics and connected components of $\Omega \setminus L$. There are two important properties of a minimal configuration: the graph G has no loops (i.e. it is a collection of its connected components that are trees), and each vertex that is a leaf in some tree is a vertex of some geodesic. With these properties, one proceeds to label all geodesics in a consecutive order, with $\tau_1 \preceq \ldots \preceq \tau_N$. Here, $\tau_r \preceq \tau_{r+1}$ means that the concatenated polygonal curve from O_1 to O_2 via τ_r and then back to O_1 via τ_{r+1} encloses a region D_r and it is oriented counterclockwise with respect to D_r. Next, one labels and orders the trees $\{T_m\}_{m=1}^s$ in $\bar{D}_r$ so that $D_r \setminus L$ is partitioned into subregions $\{P_m\}_{m=0}^s$ and $\{Q_m\}_{m=1}^s$ in the following way: each P_m is a polygon bounded by the "right most" path from the tree T_m, the "left most" path from T_{m+1}, and the intermediate portions of τ_r and τ_{r+1} which are concave with respect to P_m. Each Q_m is a finite union of polygons enclosed within the single tree T_m, again bounded by the intermediate portions of geodesics τ_r and τ_{r+1}. Note that τ_r and τ_{r+1} may have nontrivial overlaps and some of $\{Q_m\}_{m=1}^s$ may be absent.

Step 3: Constructing a desired isometric immersion. Finally, we fix the segment $I = [0, l_g]$ along the x_1-axis in $\mathbb{R}^3$. To construct an isometric immersion u of $\Omega \setminus L$ such that $u(O_1) = 0$, $u(O_2) = l_g e_1$, $u(\tau_r) = I$ for $r = 1, \dots, N$, and where each segment on τ_r is mapped onto a designated segment portion of I, we first note that u consists exclusively of planar folds and returns the image that is a subset of $\mathbb{R}^2$. By *Step 2*, $D_r = \bigcup_{m=0}^s P_m \cup \bigcup_{m=1}^s Q_m$, for $r = 1, \cdots, N-1$, so that it is possible to construct u on $P_0, Q_1, Q_2, \dots, Q_m, P_m$, even though the step to construct u on $P_1, \dots, P_{m-1}$ can be highly technical [16]. Since the exterior region $D_0 = \Omega \setminus \bigcup_{r=0}^{N-1} D_r$ does not contain trees, the two outermost geodesics σ_1 and σ_N are convex, and so the definition of u on D_0 consists of several simple folds. We note that the condition $O_1, O_2 \in \partial\Omega$ is essential here: indeed there exist minimal configurations for $O_1, O_2 \notin \partial\Omega$, that do not admit any isometry u with the property that the Euclidean distance from $u(O_1)$ to $u(O_2)$ equals the geodesic distance from O_1 to O_2 in $\Omega \setminus L$ (for further details, we refer to [16]).

5. Functional kirigami structures

The geometric mechanics of ordered and disordered kirigami leads us naturally to questions of design for function. We apply the principles discussed so far to three examples: a soft gripper with multiple modes of grasping, a family of kirigami designs displaying optical transmittance and shielding properties, and a physically unclonable function based on the inherent disorder in the deformation of kirigami sheets.

(a) Active and passive gripping

The opening of a kirigami slit upon loading suggests its potential as a soft grasper, its shape modulated by an applied force or strain at the boundary [12,18]. To be effective, a grasper

must enable controlled gripping, lifting and relocating objects of varying scales and shapes with minimal energy input.

We define a passive grasper as one that only requires external work to be done in order to grasp or release the object, with *energy-free* relocation while an active grasper requires continuous application of an external force (external energy) to grasp and relocate, as shown in the schematics in figure 7*b*,*c*. Kirigami enables both designs; while the active grasper accommodates the target object in the curved features of the deformed sheet, the passive grasper uses the cuts to accommodate objects.

The simplest passive grasper design, a single slit perpendicular to the loading axis, requires a prestretch to deform the cut into a hole that can accommodate the target object. On releasing the prestretch, the cut boundary relaxes to contact the object, grasping it with no further energy input. After relocation, the arrested object can be released by applying an extensional strain to the sheet.

However, a potential drawback of this solution is that the object is liable to rotate in order to accommodate the two point-like forces from the cut edge on either side. Our disordered kirigami observations suggest adding more cuts softens the grasper's loading curve, enabling symmetric deformation and reducing the severity of sudden reorientations at a minor cost to the maximum load bearing capacity. Hence, an effective design of a kirigamized grasper is one that has multiple smaller cuts in addition to a larger cut in the middle as shown in figure 7*a*. The additional cuts are prescribed in a way that all cuts have a PR = 1, and buckle under the applied strain. Further, the largest cut is split in the middle by a small cut, oriented along the pulling axis. Together these features enable symmetric deformation of the flat kirigami sheet, and improve the stability of contact with the grasped object. The additional contact points may not help stabilize the grasped object if the size of the object is much smaller than that cut length, in which case the grasped object may slip during handling. We note that the simplest kirigamized grasper with a single cut (figure 2*a*) deforms asymmetrically, and hence cannot be effectively used as a grasper in both active and passive modes. In practical scenarios however symmetric deformation can be realized if the sheet is stretched significantly [19].

The final design sequence is demonstrated in figure 7*b*,*c* and visualized in the electronic supplementary material, movie S3. In this passive mode, the conical tips and the cylindrical core of the kirigami sheet enables confinement of the target object as shown in figure 7*b* and electronic supplementary material, movie S3. The same geometry also functions as an active grasper, as the two ends of the middle cut are forced toward each other as loading is applied. For the symmetric deformations, this may be used to encase an object with compressive force and relocate it, as shown in figure 7*c*.

The range of applicability of a general kirigami grasper can be understood from a balance of the forces due to the bending of kirigami sheet, and the weight of the grasped object. For a cut of length l, the characteristic grasping force of the deformed sheet can be written as $f_g \sim \mu(B/l)c(\gamma)$, with μ being the coefficient of friction and $c(\gamma)$ is a strain-dependent geometric factor. For an object with effective density ρ and size l, force balance yields $\mu(B/l)c(\gamma) \sim \rho g l^3$. This provides a non-dimensional parameter $\rho g l^4/(\mu B c(\gamma))$, which has values ranging between 1 and 100 for the successful grasping demonstrations we attempted using a plastic grasper. For a kirigami gripper with an arbitrary configuration of cuts, the geometric and mechanical response of kirigamized sheets in various ordered and disordered cases can help estimate the non-dimensional kirigami grasper parameter. This is because the nature of force–strain curve for ordered/disordered kirigami is universal (schematics in figure 7*b*,*c*) and knowing the force in the extensible regime, i.e. force corresponding to points 1, 3 in figure 7*b* and point 2 in figure 7*c*, will help determine the operating regime of the gripper.

(b) Selective transmittance

Although our discussion so far has been restricted to piecewise linear cuts, the ideas established are applicable to cuts with finite planar curvature. Inspired by the recent efforts towards

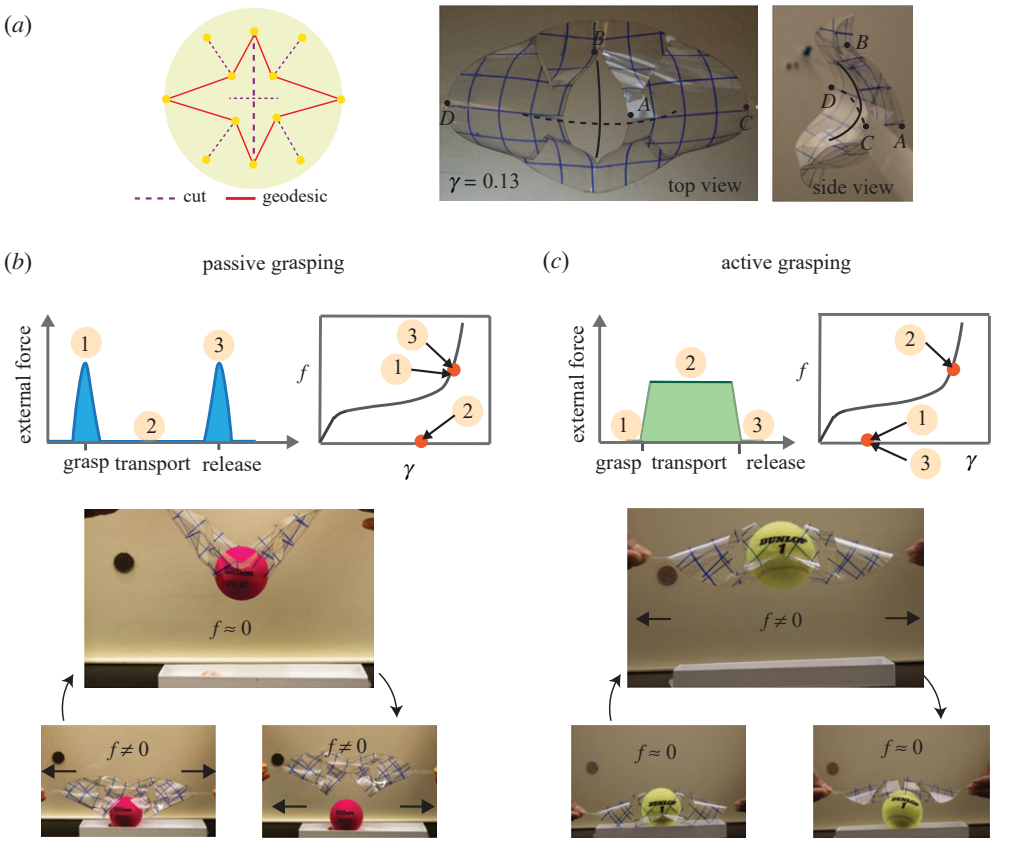

Figure 7. A kirigami grasper. (*a*) A kirigami design for grasping objects. The deformed sheet shows the concave regions (for active grasping), and open holes (for passive grasping). (*b*) The kirigami grasper can be employed in passive and active modes requiring different energy input, shown in (*b*) and (*c*), respectively. The experimental images depict the passive grasping of a racquet ball and active grasping of a tennis ball.

design of kirigami-based mechanically deployable structures [1], we demonstrate a family of deployable kirigami designs whose force-dependent transmittance properties can be tuned by varying a single geometric parameter. The application follows directly from our observations (in figures 2–5) and analysis in figure 6 that with the increasing strain the geodesic in kirigamized structures straightens out and the cuts with PR = 1 localize the bending deformation. Thus, a careful choice of cuts (and hence the geodesic) can be used to embed force/strain-dependent functional features in kirigamized sheets.

Figure 8*a* shows three cases of physical kirigamized sheets perforated with five concentric circular arcs, differing only by a parameter $\mathrm{d}\phi$ that defines the arcuate cuts that extend between $\pm\mathrm{d}\phi$ and $\pm(\pi - \mathrm{d}\phi)$ with respect to the vertical axis, while the radius is linearly increased between the five arcs. We see that the planar kirigami sheets (with marginally different $\mathrm{d}\phi$) show very different geometric mechanics under a small applied strain. When $\mathrm{d}\phi = \pi/60$, none of the cuts intersect the vertical diameter, leaving a straight geodesic connecting O_1 and O_2; hence, tensile loading of this structure results in simple in-plane stretching along this diameter.

However, a small change in $\mathrm{d}\phi$ to $-\pi/180$ results in each of the circular cuts now intersecting the vertical diameter, resulting in a geodesic connecting O_1 and O_2 that must meander around the corners of all cuts. Under an applied load, this structure shows a large relative out-of-plane displacement of different domains of the sheet (see electronic supplementary material, movie S4). Further increasing the angular extent of the cuts by taking $\mathrm{d}\phi = -\pi/30$ makes the geodesic

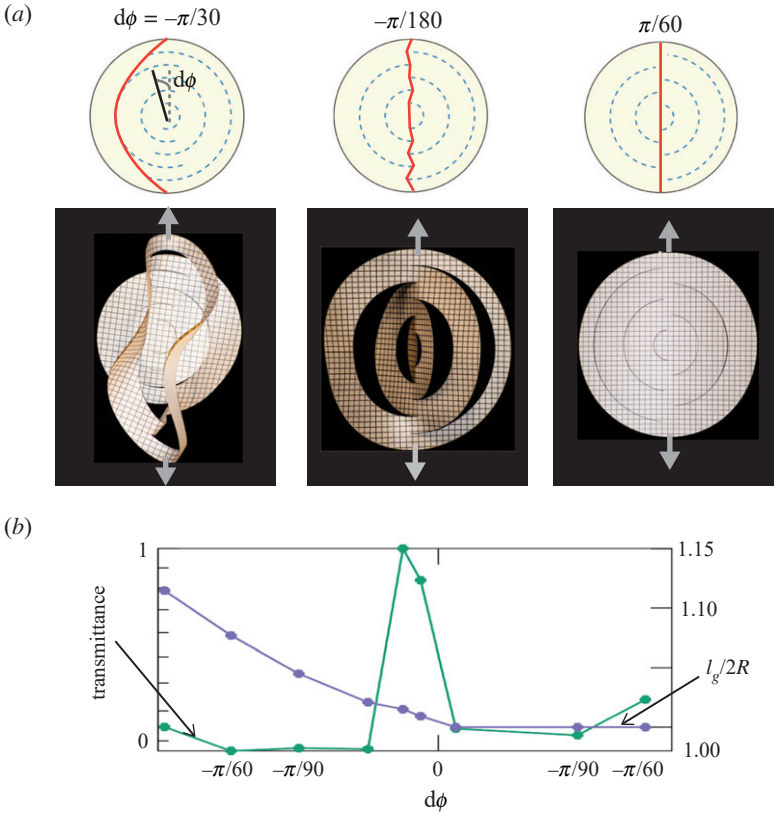

Figure 8. A kirigami light window. (*a*) Experimental images of kirigami sheets with circular curved cuts (dashed lines on top row) show very different responses to an applied strain when the cut geometry is varied. Red curves represent the geodesic connecting loading points O_1 and O_2, which changes dramatically as the curved cuts are very slightly extended or shortened near the vertical diameter. dϕ represents the angular deviation of each cut's endpoint with respect to this vertical diameter. When d$\phi > 0$, the geodesic is simply the diameter connecting the loading points. However, when the cuts begin to intersect this diameter for d$\phi < 0$, the geodesic must take a different path and significantly alters the deployed geometry. Physical parameters are identical to those in figure 1. (*b*) A phase diagram quantifying the transmittance (left axis) of the deployed kirigami structures in varying the parameter dϕ, subject to strain of 1%. Transmittance of the kirigami window is quantified as the relative change in the projected area of deformed sheet on the rest plane. The right axis reports geodesic distance normalized by sheet diameter, $l_g/2R$.

qualitatively change, as it now skirts the two outermost cuts without intersecting any of the inner cuts. Since the inner cuts have PR = 0, and hence do not introduce any soft deformation modes, under an applied deformation, the outer frame localizes the bending while the inner structure stays nearly planar without any deformation, and is thus shielded mechanically and geometrically.

We now quantify some of the functional responses of these kirigamized structures using dϕ as the only tunable parameter. A straightforward observation is that the force required to deform such a class of structures increases monotonically with dϕ (see electronic supplementary material, figure S11*a*). Very different geometric consequences due to changing geodesic paths can be quantified in terms of the *transmittance* of the kirigami structure. In practice, transmittance may correspond to the light transmitted though an optical window when illuminated with light rays perpendicular to the rest plane. In experiments, we restrict the deformation to small strains approximately 1%, a practically relevant regime, and note that geometric mechanics are generally strain-dependent.

Figure 8*b* shows a phase diagram of transmittance (left axis) measured at 1% strain as a function of dϕ, along with the computed geodesic length normalized by diameter ($l_g/2R$) for reference. The transmittance curves clearly display non-monotonic trends. *Transmittance* is achievable in the cases when $l_g \to 2R$, and the strain sensitivity of transmittance is enhanced with increasing $l_g/2R$ (see electronic supplementary material, figure S11*b*). For cases with d$\phi > 0$, we note $l_g/2R = 1$ and we see only weak variation of *transmittance*, since these structures must deform primarily by planar stretching.

(c) Kirigami-based physically unclonable function

We close with an unusual application of kirigami for encoding information, inspired by the fact that for a given configuration of cuts in a sheet, every choice of a loading axis 'activates' a distinct set of deformations anchored at different cuts (i.e. cuts with PR $\neq 0$), each leading to a distinct geometrical response. Such a system in principle can be employed to encrypt information geometrically in a flat kirigamized sheet. Encoding information in such a system involves a choice of the number of cuts (N), parameters associated with each cut (x_i, y_i, l_i and θ_i), a loading axis, and an extensional strain γ. The resulting high-dimensional design space leads to a rich nonlinear strain-dependent and possibly discontinuous shape response.

This observation allows us to use kirigami sheets that are easy to realize practically in creating physically unclonable functions (PUFs), building on the notion that the inherent disorder in many physical systems is a promising hardware route towards roots-of-trust cryptographic keys [20,21]. Specifically, a kirigami PUF is generated by activating/stretching a kirigamized sheet along a loading axis up to a fixed nominal strain. The deformed sheet is then imaged with a camera held at a fixed distance and orthogonal to the initial plane of the sheet, and a z-displacement map is created for the deformed structure. We store this z-displacement map, i.e. $|z|$ as a PUF key. For future authentication, the user will need to know the cut configuration, loading axis and the extensional strain to duplicate such a key. Figure 9*a* shows a planar kirigamized sheet with disordered cuts, and figure 9*b* shows the greyscale z-displacement maps of the kirigami structure for different strain values and a different choice of loading axis. Since we use a two-dimensional z-displacement map as a PUF key, we rely on a measure of image similarity index to match keys between different experiments. Here, we use the multiscale structural similarity index function in MATLAB [22] to compare different keys. The index quantifies the luminance, contrast and structure of several versions of the image at various scales, with its values ranging between 0 and 1 (1 being the highest possible match).

To demonstrate the effectiveness of kirigami as a PUF in a minimal setting, we keep the cut configuration of the kirigamized sheet fixed and only vary the loading axis and the applied strain. The versatility of the kirigami PUF is directly linked to the nonlinear geometric mechanics of disordered kirigami, and our observations make it evident that kirigamized sheets will yield a deterministic geometric mechanical response. Thus given complete information about all the variables involved, the PUF key will be deterministic. In practice, having a large number of cuts will make it very difficult to be reverse engineered by an adversary.

A robust PUF system will return significantly different (false) PUF keys if there exists a mismatch between the loading axis and the applied strain that corresponds to the stored (true) PUF key, because even a small variation in the loading axis by dθ results in a sharp decrease in the key similarity as shown in figure 9*c*. As an example, setting a threshold value on the similarity index to 0.9 will enable a robust response from this PUF system, and yet allows for a margin of error in $\pm$dθ. In figure 9*d*, we show that there is a similar robustness in the PUF keys when the applied extensional strain is varied. Indeed, we see that kirigami-based PUF are only effective when the strain is large enough for the structure to undergo substantial out-of-plane deformation and corresponds to the plateau regime in the force–displacement curve. In the vicinity of the strain corresponding to the stored key, a slight error in the applied strain does not impact the PUF performance, while a significant deviation results in a poor match.

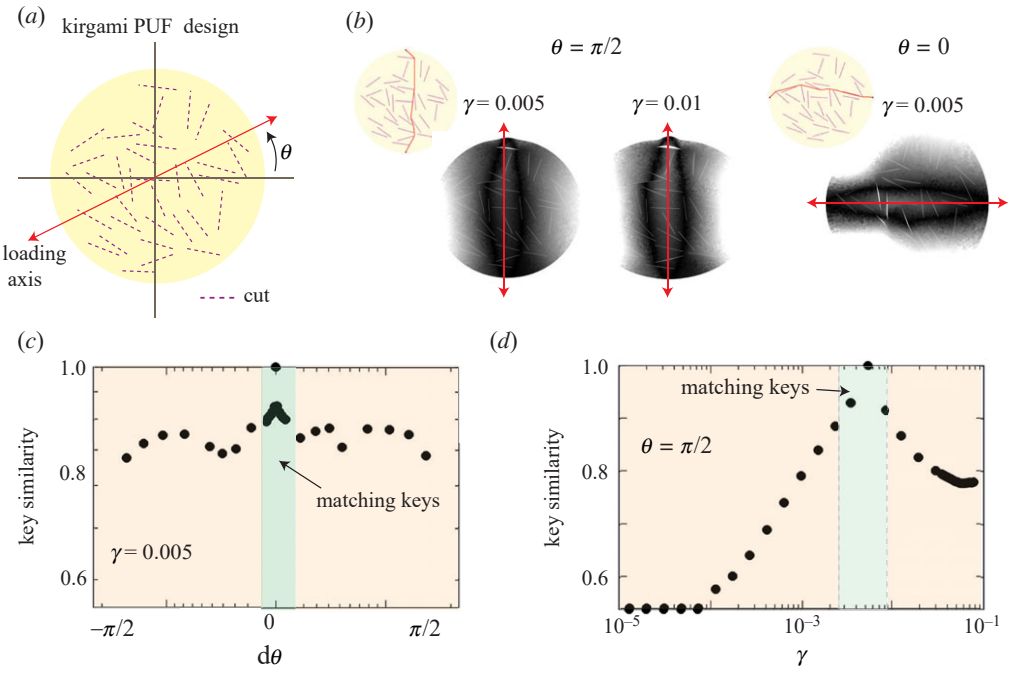

Figure 9. A kirigami approach for geometric encryption. (*a*) A physically unclonable function (PUF) can be realized using kirgamized sheets. For a given configuration of disordered cuts, loading axis and tensile strain, a unique three-dimensional deformation is realized. The *z*-deformation map of the kirigamized structure is used as a PUF at a fixed γ and θ. (*b*) Examples of PUF keys that can be realized using the kirigamized sheet in (*a*) for various strains γ and loading angle θ. The geodesics for each of the cases overlaid on the cut pattern is also shown. (*c*) A change in the loading axis (large dθ) results in PUF keys that are quantitatively different due to the changing geometric mechanics of kirigamized sheets (highlighted red). A slight mismatch (small dθ) between the loading axis yields keys which show high similarity to the stored key (highlighted in green). (*d*) The PUF keys are robust to small change in the strain (highlighted green), keeping the cut configuration and loading axis fixed, while a large change in applied strain leads to significantly different PUF keys (highlighted in pink).

6. Discussion

Our study of ordered and disordered kirigami has shown how elementary geometric and energetic concepts allow us to understand the three-dimensional structure and mechanical response of kirigamized sheets. The general principles relating the mechanical response of such sheets to their geometry, along with scaling arguments for all regimes of deformation, reduces a complex nonlinear problem to a combination of simple geometrical constructions, potentially easing the search for novel kirigami-based engineering solutions in instances such as grasping, windowing and encoding information. We believe that these examples are just the beginning of a different way of thinking about functional aspects of topological and geometrical mechanical metamaterials.

Data accessibility. Code for our numerical simulations are available from the GitHub repository: https://github.com/jeffersontide/kirigami2022.

The data are provided in electronic supplementary material [23].

Authors' contributions. G.C. and L.N. contributed equally. G.C.: conceptualization, data curation, formal analysis, investigation, methodology, software, validation, visualization, writing—original draft, writing—review and editing; L.N.: conceptualization, data curation, formal analysis, investigation, methodology, software, validation, visualization, writing—original draft, writing—review and editing; M.L.: formal analysis, investigation; Q.H.: formal analysis, investigation; L.M.: conceptualization, formal analysis, funding acquisition, investigation, methodology, project administration, supervision, validation, writing—original draft, writing—review and editing.

All authors gave final approval for publication and agreed to be held accountable for the work performed therein.

Conflict of interest declaration. We declare we have no competing interests.

Funding. The work was supported partially by NSF grant no. DMS-2006439 (M.L.), BioMatter DMR 1922321 (L.M.), MRSEC DMR 2011754 (L.M.), EFRI 1830901 (L.M.), the Simons Foundation (L.M.) and the Seydoux Fund (L.M.), the NSF-Simons Center for Mathematical and Statistical Analysis of Biology at Harvard, award no. 1764269 and the Harvard Quantitative Biology Initiative (L.N., L.M.).

References

1. Zhang Y *et al.* 2015 A mechanically driven form of kirigami as a route to 3D mesostructures in micro/nanomembranes. *Proc. Natl Acad. Sci. USA* **112**, 11 757–11 764. (doi:10.1073/pnas.1515602112)
2. Blees MK *et al.* 2015 Graphene kirigami. *Nature* **524**, 204–207. (doi:10.1038/nature14588)
3. Bertoldi K, Vitelli V, Christensen J, Van Hecke M. 2017 Flexible mechanical metamaterials. *Nat. Rev. Mater.* **2**, 1–11. (doi:10.1038/natrevmats.2017.66)
4. Rafsanjani A, Bertoldi K. 2017 Buckling-induced kirigami. *Phys. Rev. Lett.* **118**, 084301. (doi:10.1103/PhysRevLett.118.084301)
5. Moshe M, Esposito E, Shankar S, Bircan B, Cohen I, Nelson DR, Bowick MJ. 2019 Kirigami mechanics as stress relief by elastic charges. *Phys. Rev. Lett.* **122**, 048001. (doi:10.1103/PhysRevLett.122.048001)
6. Sadik S, Dias MA. 2021 On local kirigami mechanics I: isometric conical solutions. *J. Mech. Phys. Solids* **151**, 104370. (doi:10.1016/j.jmps.2021.104370)
7. Choi GPT, Dudte LH, Mahadevan L. 2019 Programming shape using kirigami tessellations. *Nat. Mater.* **18**, 999–1004. (doi:10.1038/s41563-019-0452-y)
8. Choi GPT, Dudte LH, Mahadevan L. 2021 Compact reconfigurable kirigami. *Phys. Rev. Res.* **3**, 043030. (doi:10.1103/PhysRevResearch.3.043030)
9. Love AEH. 2013 *A treatise on the mathematical theory of elasticity*. Cambridge, UK: Cambridge University Press.
10. Khoklov AR, Grosberg AY, Pande VS. 1994 *Statistical physics of macromolecules*, Vol. 1. New York, NY: AIP Press.
11. Prager W. 1957 On ideal locking materials. *Trans. Soc. Rheol.* **1**, 169–175. (doi:10.1122/1.548818)
12. Dias MA, McCarron MP, Rayneau-Kirkhope D, Hanakata PZ, Campbell DK, Park HS, Holmes DP. 2017 Kirigami actuators. *Soft Matter* **13**, 9087–9092. (doi:10.1039/C7SM01693J)
13. Isobe M, Okumura K. 2016 Initial rigid response and softening transition of highly stretchable kirigami sheet materials. *Sci. Rep.* **6**, 1–6. (doi:10.1038/srep24758)
14. Inglis CE. 1913 Stresses in a plate due to the presence of cracks and sharp corners. *Trans. Inst. Naval Archit.* **55**, 219–241.
15. Zehnder AT, Potdar YK. 1998 Williams meets von Karman: mode coupling and nonlinearity in the fracture of thin plates. *Int. J. Fract.* **93**, 409–429. (doi:10.1007/978-94-017-2854-6_21)
16. Han Q, Lewicka M, Mahadevan L. 2022 Isometric immersions with rectifiable geodesics. Accepted, *Rocky Mountain Journal of Mathematics*.
17. Kawasaki T. 2005 *Roses, origami & math*. Tokyo: Japan Publications Trading.
18. Hong Y, Chi Y, Wu S, Li Y, Zhu Y, Yin J. 2022 Boundary curvature guided programmable shape-morphing kirigami sheets. *Nat. Commun.* **13**, 530. (doi:10.1038/s41467-022-28187-x)
19. Yang Y, Vella K, Holmes DP. 2021 Grasping with kirigami shells. *Sci. Rob.* **6**, eabd6426. (doi:10.1126/scirobotics.abd6426)
20. Pappu R, Recht B, Taylor J, Gershenfeld N. 2002 Physical one-way functions. *Science* **297**, 2026–2030. (doi:10.1126/science.1074376)
21. Gao Y, Al-Sarawi SF, Abbott D. 2020 Physical unclonable functions. *Nat. Electron.* **3**, 81–91. (doi:10.1038/s41928-020-0372-5)
22. Wang Z, Simoncelli EP, Bovik AC. 2003 Multiscale structural similarity for image quality assessment. In *The 37th Asilomar Conf. on Signals, Systems & Computers, 2003, Pacific Grove, CA, USA*, vol. 2, pp. 1398–1402. IEEE.
23. Chaudhary G, Niu L, Han Q, Lewicka M, Mahadevan L. 2023 Geometric mechanics of ordered and disordered kirigami. Figshare. (doi:10.6084/m9.figshare.c.6631833)